Impact of Chlorine Functionalization on High-Mobility Chemical Vapor Deposition Grown Graphene

Xu Zhang,[†] Allen Hsu,[†] Han Wang,[†] Yi Song,[†] Jing Kong,[†] Mildred S. Dresselhaus,[†,‡,*] and Tomás Palacios[†,*]

[†]Department of Electrical Engineering and Computer Science, Massachusetts Institute of Technology, Cambridge, Massachusetts 02139, United States and [‡]Department of Physics, Massachusetts Institute of Technology, Cambridge, Massachusetts 02139, United States

ABSTRACT We systematically investigated plasma-based chlorination of graphene and compared its properties before and after such treatment. X-ray photoelectron spectroscopy revealed that a high Cl coverage of 45.3% (close to C_2Cl), together with a high mobility of 1535 $cm^2/(V\ s)$, was achieved. The C:Cl ratio n (C_nCl) can be effectively tuned by controlling the dc bias and treatment time in the plasma chamber. Chlorinated graphene field-effect transistors were fabricated, and subsequent Hall-effect measurements showed that the hole carrier concentration in the chlorinated graphene can be increased roughly by a factor of 3. Raman spectra indicated that the bonding type between Cl and graphene depends sensitively on the dc bias applied in the plasma chamber during chlorination and can therefore be engineered into different reaction regimes, such as ionic bonding, covalent bonding, and defect creation. Micro-Raman mapping showed that the plasma-based chlorination process is a uniform process on the micrometer scale.

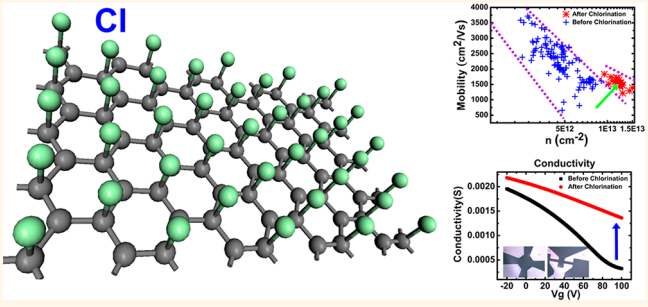

KEYWORDS: graphene · functionalization · chlorination · mobility · coverage · Raman spectroscopy · controllability

Graphene, a zero-gap semiconductor with massless charge carriers, has attracted tremendous interest in the scientific community, owing to its unique linear band structure and remarkable mechanical and electronic properties.[1−3] One of its very special properties is that graphene is an all-surface material; therefore, every atom has access to the surface, which has a direct impact on its electronic and chemical performance. Surface functionalization of graphene through hydrogenation and fluorination has been widely investigated,[4−8] and new graphene derivatives with novel properties, such as band-gap opening,[6,9,10] controllable doping,[11−13] and edge passivation,[14] have been successfully created. It is worth noting that a high fluorine (F) coverage on graphene has been achieved: it saturates at 25% (atomic) for single-sided graphene and reaches 100% when both sides of graphene are exposed. Also, graphane, with 100% H coverage on graphene, was first theoretically studied by Sofo *et al.*[15] and experimentally realized by Elias *et al.* in 2009.[4]

Recently, chlorinated graphene has also been achieved and studied by different approaches.[16−19] Theoretical calculations, based on density functional theory (DFT), showed that chlorine atoms interact with graphene in a very different way from the H or F cases.[20,21] For hydrogenation and fluorination, the interaction between graphene and H/F is always through the formation of covalent C−H/C−F bonds. However, in chlorinated graphene, various bonding types are possible, and therefore richer phenomena are expected. Moreover, in the double-sided fully chlorinated graphene (CCl), a band gap up to 1.21 eV is predicted by first-principles DFT calculations.[20] Previous experimental work showed that photochemical chlorination can form C−Cl covalent bonds and make graphene highly resistive, with about 8% (atomic) chlorine coverage.[16] It has also been successfully demonstrated, by Wu *et al.*, that chlorine plasma can dope graphene p-type and can increase its conductivity, and the chlorine coverage was also determined to be about 8.5%.[17] Until now, the chlorine coverage achieved

* Address correspondence to tpalacios@mit.edu; millie@mgm.mit.edu.

Received for review May 27, 2013 and accepted July 3, 2013.

Published online July 03, 2013
10.1021/nn4026756

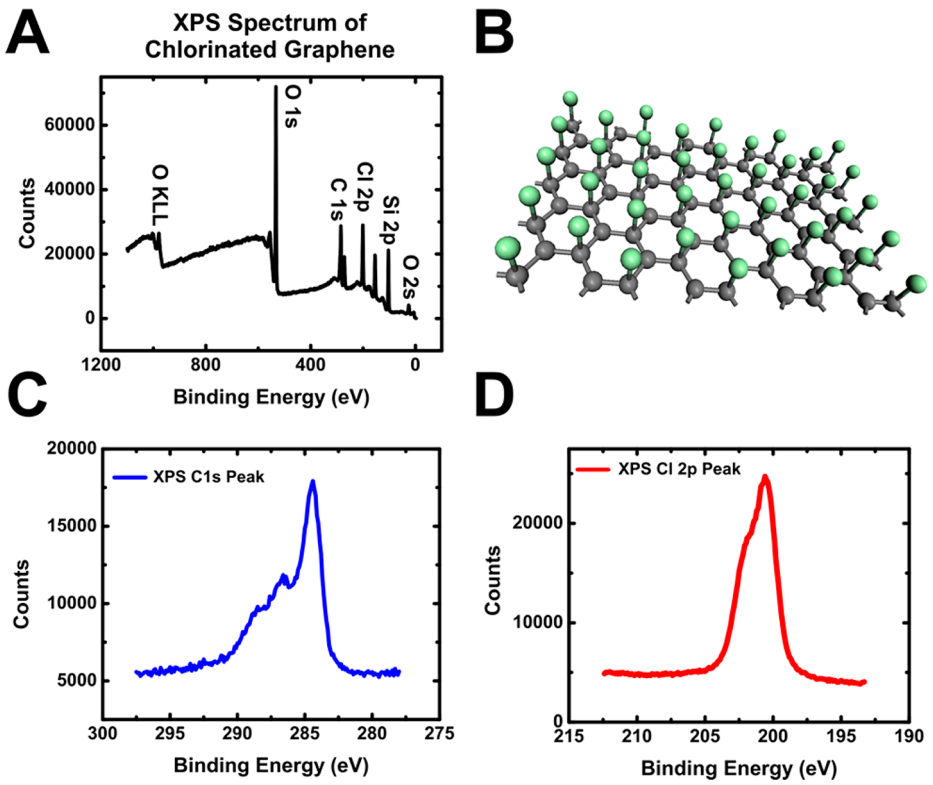

Figure 1. (A–C) X-ray photoelectron spectroscopy (XPS) characterization of the chlorinated graphene. The graphene samples were treated in Cl_2 plasma with dc bias of 8 V for 30 s. (A) Full XPS spectrum of the sample. (B) Schematic representation of the atomic structure of chlorinated graphene with a C:Cl ratio of 2:1. (C) Zoom-in view of the C 1s peak of (A). (D) Zoom-in view of the Cl 2p peak of (A).

experimentally has still been much lower than the corresponding value in the fluorination and hydrogenation cases.[4,5,9] Yang *et al.* argued that forming hexagonal Cl rings on the single-sided graphene is the most energetically stable configuration, and therefore the maximum Cl coverage is expected to be less than 25%.[21] However, there is still a discrepancy between experimental and theoretical studies.[16,17,20,21] Furthermore, previous chemical modifications, including the different hydrogenation, fluorination, and photochemical chlorination processes, result in a significant degradation of the high mobility in graphene.[4,5,16] It is of great importance to find an effective chemical functionalization method that can realize high Cl coverage while not significantly sacrificing the high mobility of the pristine graphene.

In the present work, we focus on a plasma-based chlorination process. By carefully tuning the plasma condition, we find an optimized reaction regime where we can achieve stable single-side chlorinated graphene with a high surface coverage (45.3 at. %, close to C_2Cl) and with excellent carrier mobility performance (1535 $cm^2/(V\,s)$, when the carrier concentration is around 1.2×10^{13} cm^{-2}). To the best of our knowledge, this Cl coverage is the highest presently in published results for chlorinated graphene with high mobility. X-ray photoelectron spectroscopy (XPS) and transport characterization reveal the change in the electronic properties of our samples. We also investigate the uniformity and controllability of this plasma-based chlorination method. It is demonstrated here that the dc bias applied in the plasma chamber is very effective for tuning the C:Cl ratio, and, at the same time, the interaction between the graphene and chlorine atoms can be controlled to be through ionic bonding, covalent bonding, or defect creation regimes. The reaction mechanism of the plasma-based chlorination process is also analyzed.

RESULTS AND DISCUSSION

We confirmed the existence of chlorine species on graphene and further quantified the Cl coverage on the surface by use of XPS. By carefully controlling the electron cyclotron resonance (ECR) power, dc bias, and the reaction time, the highest coverage we have achieved was 45.3%, *i.e.*, $C_{2.2}Cl$ (this quantitative analysis is based on the peak area ratio of C 1s and Cl 2p peaks and their sensitivity factors in XPS measurements). The dc bias we used was 8 V, and the treatment time was 30 s (more details in the Experimental Methods section). Figure 1A shows the full XPS characterization spectrum of our chlorinated graphene samples. The detailed C 1s and Cl 2p peaks are illustrated in Figure 1C and D, respectively. Our result is very close to C_2Cl, in which one chlorine atom is shared by two carbon atoms of one graphene unit cell, as illustrated in Figure 1B. In order to

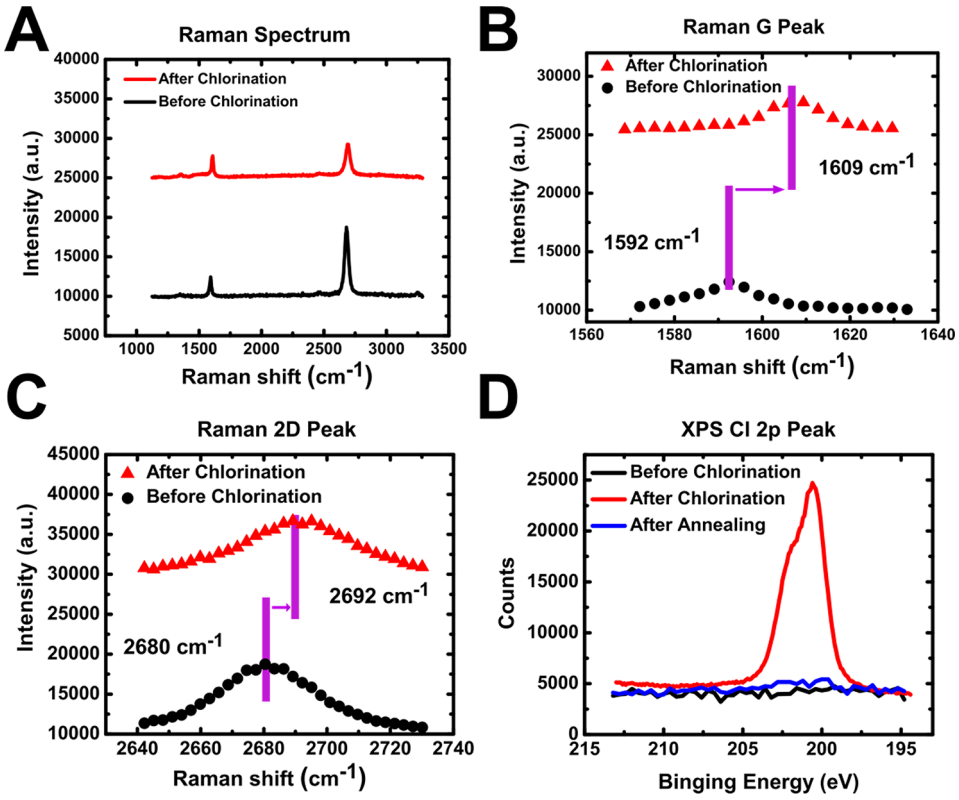

Figure 2. (A) Changes in the Raman spectra of graphene/SiO_2 caused by chlorination. The graphene sample was chlorinated in a Cl_2 plasma for 30 s, under dc bias = 8 V. (B) Zoom-in spectrum of the Raman G peak in (A). After chlorination, a significant blue shift (from ~1592 cm^{-1} to ~1609 cm^{-1}) in the G band frequency was observed. (C) Change in the Raman 2D peak frequency and line shape after chlorination. (D) Corresponding changes in the XPS results of the Cl 2p peak. Black, red, and blue curves correspond to graphene before chlorination, after chlorination, and after annealing.

further confirm the coverage of Cl on graphene, we also analyzed the deconvolution of the XPS C 1s spectrum and calculated the ratio of C−Cl and C−C components in the C 1s peak (see Supporting Information, Figure S1). The C−Cl and C−C bond ratio was determined to be about 42.6% by this approach (Supporting Information), which is quite close to the value of 45.3% that we calculated by the first method. It further validates the high chlorine coverage in this work. We found that this result was repeatable, and the as-fabricated sample was stable at room temperature under ambient conditions for about one week. It is worth noting that there is controversy in several theoretical papers about what is the most energetically favorable configuration for chlorinated graphene.[20,21] Some of the papers claimed that C_2Cl is not energetically stable and therefore cannot be realized in single-side chlorinated graphene, due to the strong interaction between adjacent chlorine atoms. The two adjacent Cl atoms in C_2Cl will form, the papers argue, a Cl_2 molecule first and escape, rather than bond with carbon atoms underneath.[20,21] However, our experimental results contradict those theoretical studies. More work is needed to explain the gap between experiment and theory.

Raman characterization was done to investigate how the chlorination changes the structure and properties of graphene. Figure 2A shows the evolution of the Raman spectra for the graphene samples before and after chlorination. The I_D/I_G intensity ratio was slightly increased, from 0.12 to 0.16 after chlorination. However, we found a significant blue shift in the Raman G peak from 1592 cm^{-1} to 1609 cm^{-1}, as shown in Figure 2B. Meanwhile, the Raman 2D peak also experienced a blue shift from 2680 cm^{-1} to 2692 cm^{-1} (Figure 2C). All of these observations indicate a hole doping effect during this chlorination treatment,[22] consistent with the result reported by Wu *et al.*[17] However, the 17 cm^{-1} blue shift in the Raman G peak we obtained here is significantly larger than the 3 cm^{-1} blue shift reported previously.[17]

Hall-effect measurements were carried out to further confirm the sign of the hole doping and to measure the change in the carrier concentration before and after chlorination. Figure 3 shows typical changes in transport properties of graphene induced by the chlorine plasma. First, the hole concentration n_h was increased from about 4.5×10^{12} cm^{-2} to about 1.2×10^{13} cm^{-2}, which are average values based on transport measurement of 23 chlorinated graphene devices (Figure 3A), confirming the significant hole doping effect indicated in the Raman spectrum. This can be explained by the fact that Cl has a higher electronegativity (3.16 on the Pauling scale) than C (2.55 on the Pauling scale).[23]

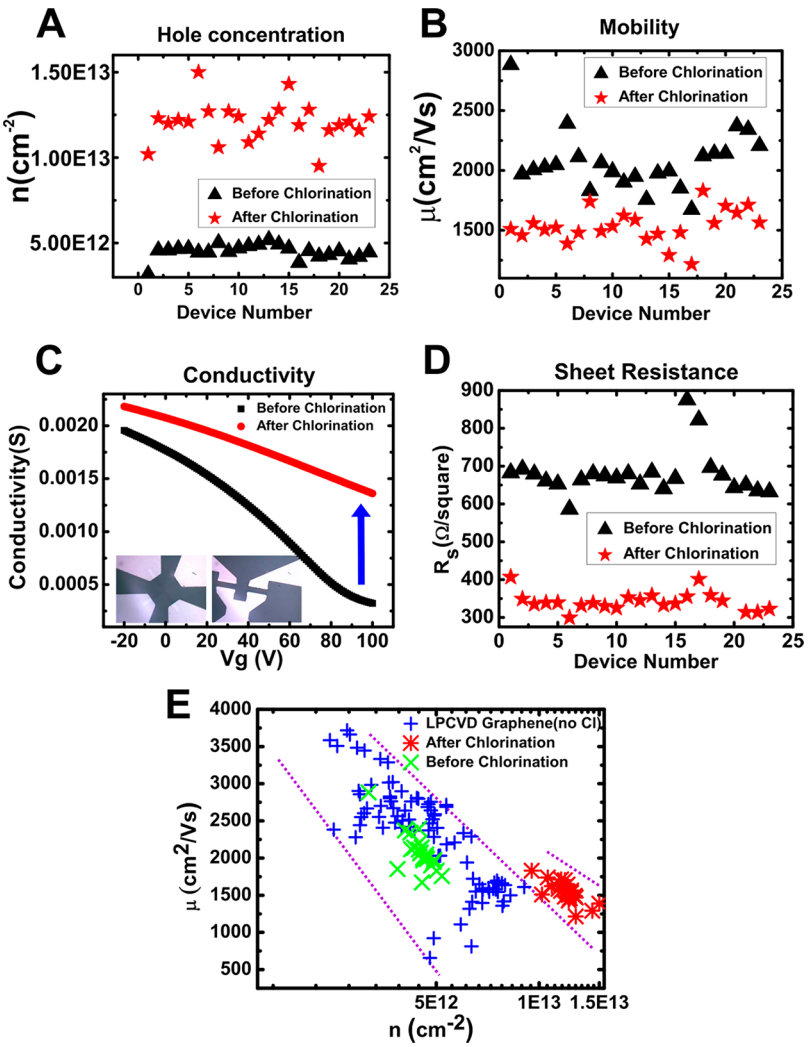

Figure 3. Changes in the transport properties of graphene after chlorination. (A) Changes in the carrier concentration n_h of 23 chlorinated graphene devices, before (black triangles) and after (red stars) chlorination. (B) Changes in mobility μ of the same chlorinated graphene devices, before (black triangles) and after (red stars) chlorination. (C) Changes in the electrical conductivity σ with gate voltage V_g shown by comparing the $\sigma(V_g)$ curves before (black) and after (red) chlorination. (Inset) Optical images of some examples of chlorinated graphene devices. The left one shows a cross-shaped graphene device for Hall-effect measurement. The right one is a chlorinated graphene field-effect transistor with 300 nm SiO_2 on doped silicon serving as a back gate dielectric. (D) Changes in the sheet resistance R_s of the chlorinated graphene devices, before (black triangles) and after (red stars) chlorination. (E) Mobility and carrier concentration data comparison (green: 23 LPCVD-grown graphene devices before chlorination, the same devices as the ones in (A)−(D); red: 23 LPCVD-grown graphene devices after chlorination, the same devices as the ones in (A)−(D); blue: a new batch of LPCVD-grown graphene devices prepared under the same conditions, but without chlorination).

Meanwhile, the carrier mobility μ decreased from 2076 $cm^2/(V\ s)$ to 1535 $cm^2/(V\ s)$ on average (Figure 3B). The changes in n_h and μ therefore had competing effects on the overall conductivity σ, according to the Drude model $\sigma = ne\mu$.[24] But the σ measurement showed an overall enhancement (Figure 3C), indicating that the major increase in n_h dominates the minor decrease in μ. Not surprisingly, the averaged value of sheet resistance was decreased from 678 Ω/□ to 342 Ω/□, as a result of chlorination (Figure 3D). We note that the chlorine plasma treatment preserved a reasonably high mobility in graphene, in contrast to hydrogenation, where the mobility was degraded from 14 000 $cm^2/(V\ s)$ to 10 $cm^2/(V\ s)$,[4] and fluorination, where the mobility dropped from 1060 $cm^2/(V\ s)$ to about 5 $cm^2/(V\ s)$ in CVD graphene.[5] It is also possible to chlorinate graphene through a photochemical process, but in this case, the mobility of the chlorinated graphene also dropped from 5000 $cm^2/(V\ s)$ to 1 $cm^2/(V\ s)$.[16] The sample damage and severe mobility degradation caused by these methods significantly limit their applications in electronic devices. We also plotted and compared the mobility μ *versus* carrier concentration n_c data for our 23 low-pressure chemical vapor deposition (LPCVD) method grown graphene devices before and after chlorination (Figure 3E). As a control, we grew a new batch of LPCVD graphene samples under the same growth conditions and plotted the μ *versus* n_h data

for these samples in blue color in Figure 3E. We found that these μ *versus* n_h data form a trend (guided by the purple dashed lines in Figure 3E), in which the mobility μ decreases as the hole concentration n_h increases. This observation can be explained by the fact that the carrier−carrier scattering will be enhanced as n_h rises, and therefore the mobility μ will be reduced. The (μ, n_h) for our 23 LPCVD-grown graphene devices (the data as shown in Figure 3A and B) before chlorination falls into the same trend as mentioned above. Surprisingly, we note that the (μ, n_h) data set for chlorinated graphene forms a trend that lies above the data trend for LPCVD graphene without chlorination; that is, the plasma-based chlorination treatment can improve the mobility performance in graphene at a given carrier concentration. This observation suggests that this Cl-plasma-based treatment is an excellent p-doping approach, from the perspective of preserving the high mobility of graphene. Our results also support the assessment that the interaction between chlorine and graphene is relatively weaker than between graphene and hydrogen or fluorine.

In order to confirm the reversibility of our chlorination process after annealing, we did XPS analysis before and after annealing. It is shown that the percent of Cl atoms on graphene before chlorination is 0.2%, which confirms that the Cl contamination from the use of $FeCl_3$ during the graphene wet transfer procedure was small and almost negligible. After chlorine plasma treatment at V_{dc} = 8 V for 30 s, the Cl coverage increased to 45.3%. Although this amount of coverage remains stable at room temperature for up to one week, it drops after annealing. For example, after annealing at 350 °C for 3 h under Ar gas flow of 1000 sccm, only 1.2% Cl was left on the graphene surface, as shown in Figure 2D and Table 1.

Interestingly, we found that by controlling the dc bias and treatment time of the plasma reaction, we can effectively tune the C:Cl ratio in chlorinated graphene (Figure 4A and B). Figure 4C shows a mapping of Cl coverage on graphene, as a function of the treatment time and dc bias applied in the plasma chamber. Surprisingly, longer treatment time in the plasma chamber resulted in a lower Cl:C ratio (Figure 4B). This result is not fully understood, but one possible reason can be that after a critical treatment time further Cl plasma bombardment may activate and break the C−Cl bonds that have already formed and thus lead to a decrease in the Cl coverage. At fixed treatment time (300 s, Figure 4A), we found that an intermediate dc bias of 8 V maximized the Cl coverage. For other

TABLE 1. Evolution of Cl Coverage on Graphene after Chlorination and after Annealing, Revealed by XPS Measurements

	Cl coverage
before chlorination	0.2%
after chlorination	45.3%
after annealing	1.2%

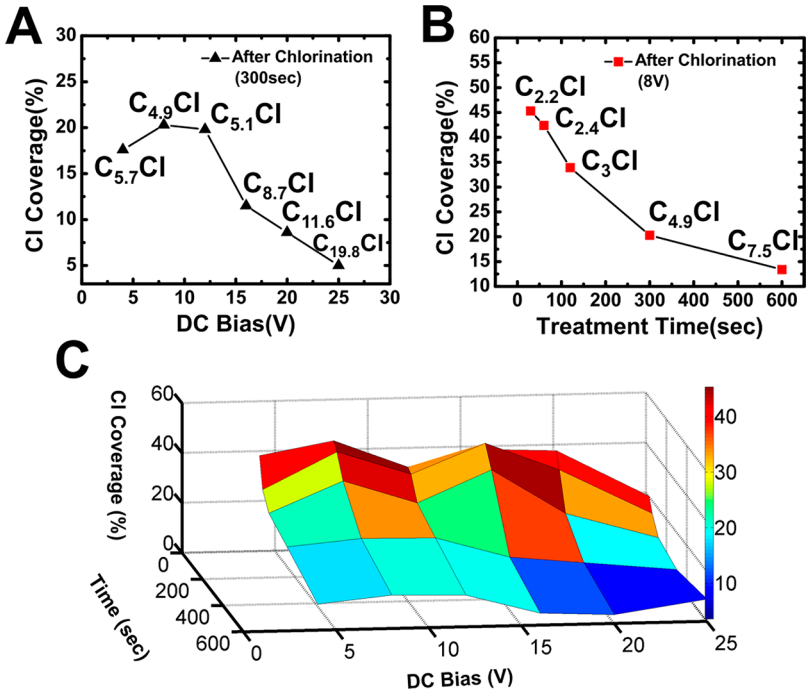

Figure 4. Controllability in the C:Cl ratio of the graphene samples chlorinated by Cl_2 plasma. (A) The C:Cl ratio changes as the dc bias applied in the plasma chamber changes. The plasma treatment time was the same (300 s) for all samples. (B) The C:Cl ratio changes with different plasma treatment times. The dc bias was maintained at a constant value (8 V) for all these samples. (C) Mapping of Cl coverage on graphene as we tuned both the plasma treatment time and dc bias applied in the chamber.

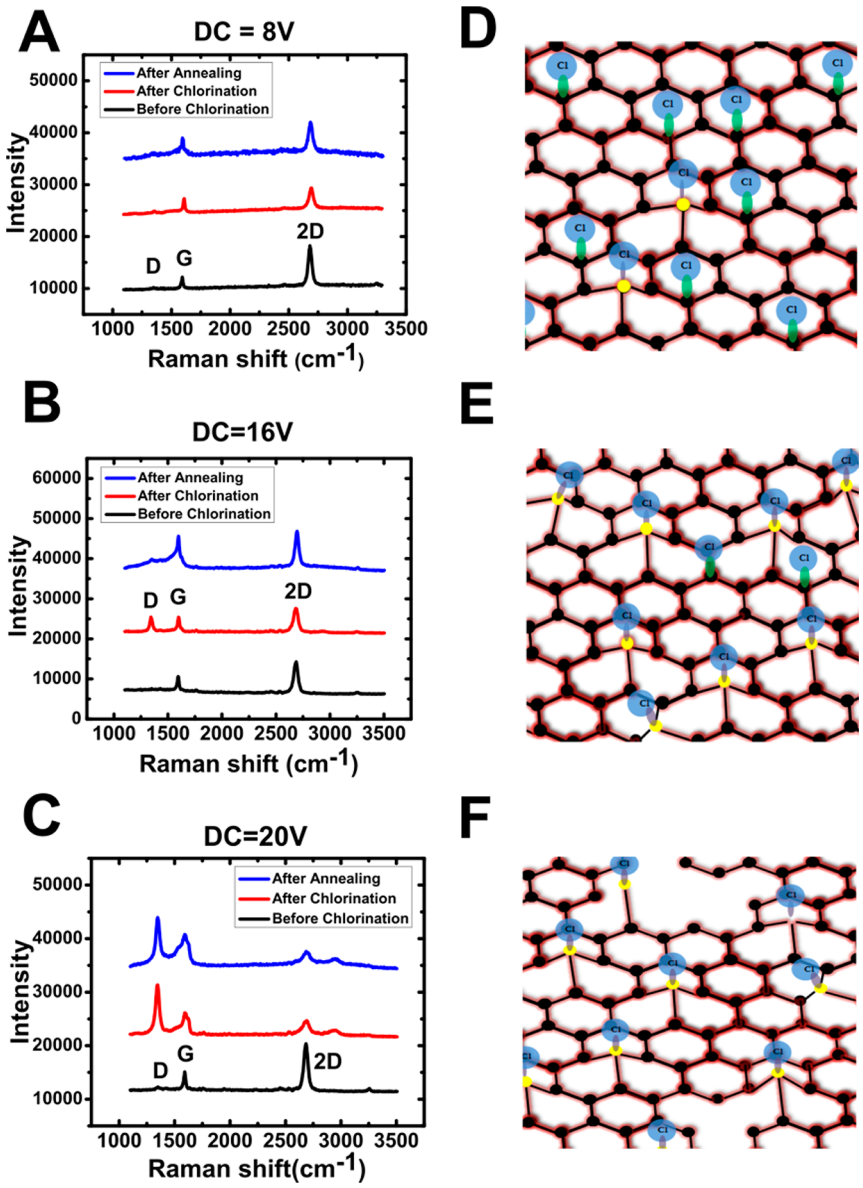

Figure 5. (A–C) Evolution of the Raman spectra of chlorinated graphene under different dc bias conditions applied in the plasma chamber. Black, red, and blue (from bottom to top) curves correspond to pristine, chlorinated, and annealed graphene, respectively. (A) V_{dc} = 8 V. Very little change occurred in the Raman D peak after chlorination. (B) V_{dc} =16 V showing a large but still mainly reversible Raman D peak that was developed after chlorination where the D band and G band intensities are similar. (C) V_{dc} =20 V showing an irreversible Raman D peak with an intensity that increased dramatically after chlorination and does not lose intensity upon annealing. (D–F) Schematic representation of the crystal structure of the chlorinated graphene under different dc bias conditions. The yellow dots indicate the carbon atoms that experience sp^2-to-sp^3 hybridization change. The light purple bonds are covalent C–Cl bonds. The black dots indicate the carbon atoms that remain in a planar structure, and the green bonds are ionic bonds between C and Cl. (D) V_{dc} = 8 V. The graphene structure largely remained planar, with mostly sp^2 C–C bonds. The carbon atoms bond with each other mainly through sp^2 hybridization bonds. (E) V_{dc} = 16 V. Some sp^3 hybridization bonds are developing with some nonplanar graphene structure. (F) V_{dc} = 20 V. Extended defects are created by the Cl_2 plasma, contributing to an irreversible Raman D peak that is not reduced in intensity by annealing.

treatment time, the optimal bias changed. For example for 60 s, we found 16 V to be the optimal dc bias condition to maximize the Cl coverage. However, a clear trend is visible that at too low (<8 V) or high (>16 V) dc biases, the Cl coverage is usually lower than for the case for an intermediate dc bias range between 8 and 16 V. This phenomenon indicates that at too low values for the dc bias the interaction between C and Cl is too weak to effectively chlorinate graphene, while at too high a dc bias, the energetic Cl plasma breaks the C–Cl bonds that have been formed, so that the Cl atoms become activated and desorb from the graphene surface.

We find that the Raman spectrum of the chlorinated graphene depends sensitively on the dc bias, as illustrated in Figure 5. At low bias, for example when V_{dc} = 8 V, the

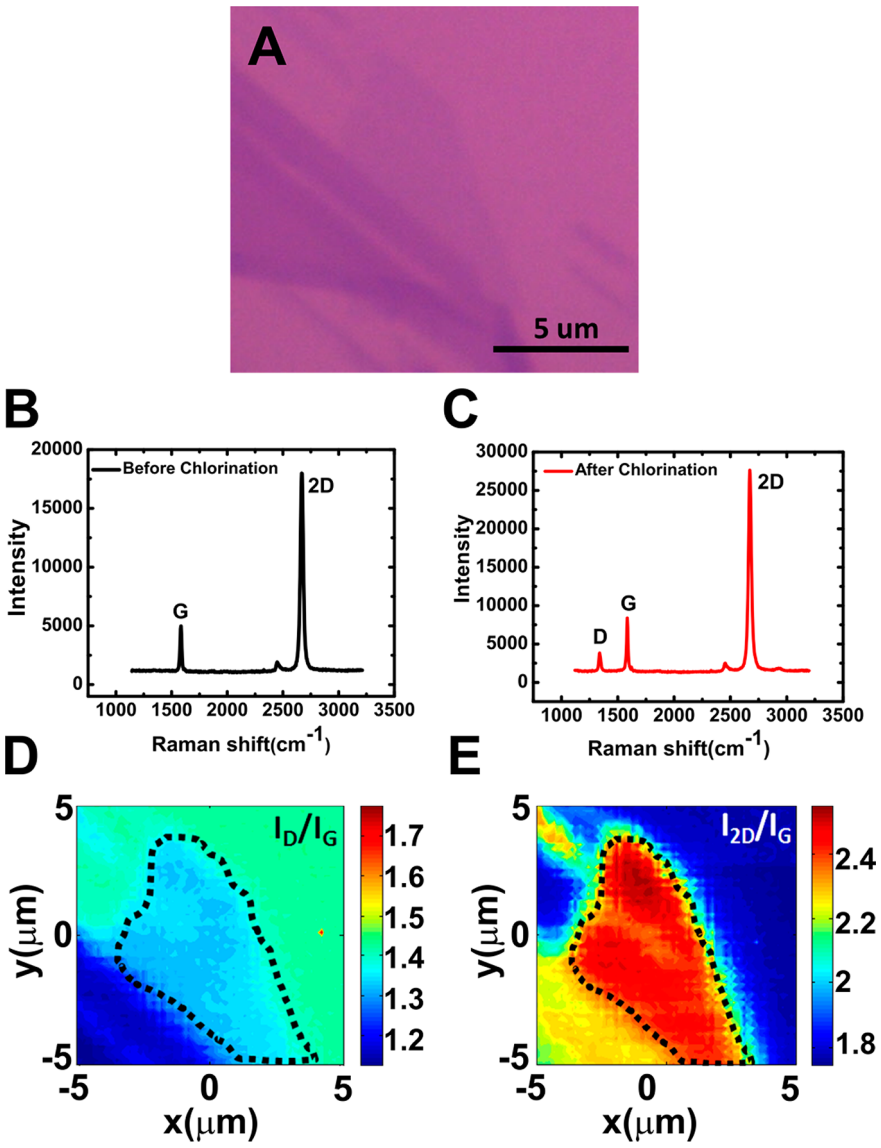

Figure 6. Investigation of the uniformity of the chlorination on a graphene surface. (A) Optical image of the exfoliated HOPG flakes. The trapezoidally shaped graphene flake (in the center area) was identified and confirmed to be monolayer graphene by Raman characterization. (B) Typical Raman spectrum of the monolayer area of the exfoliated graphene flake in (A), before chlorination. (C) Typical Raman spectrum of the monolayer area of the exfoliated graphene flake in (A), after chlorination (12 V, 300 s). (D) Raman I_D/I_G and (E) I_{2D}/I_G intensity ratio mapping of the exfoliated graphene flakes in (A). The monolayer graphene flake area is encircled by the black dash line. The color rulers to the right of (D) and (E) denote the color representation of the indicated intensity ratios.

I_D/I_G intensity ratio in the Raman spectra did not increase much after chlorination (Figure 5A). However, when the V_{dc} was increased to 16 V, the I_D/I_G intensity ratio increased substantially, from ~0 to 1.3. Importantly, this D band intensity was largely reversible under annealing: the I_D/I_G ratio dropped to only 0.3 after annealing in Ar gas at 350 °C for 3 h (too high temperature may damage graphene samples), as shown in Figure 5B. When the dc bias was further increased to 20 V, the I_D/I_G ratio increased from ~0 to 2.1, and the D band increase was irreversible, even after annealing: the I_D/I_G ratio remained at a relatively high level of 1.8 (Figure 5C). This phenomenon indicates that the interaction between the chlorine plasma and the carbon basal plane was fundamentally different under different dc bias conditions. When the dc bias was low, the intensity of the Raman D band did not increase much. Therefore, we can conclude that the symmetry in the graphene crystal structure was largely maintained with neither a major defect creation nor substantial sp^2-to-sp^3 hybridization state changes.[25,26] Meanwhile, XPS results confirmed the high coverage of Cl atoms on the graphene surface. On the basis of these observations, the interaction between Cl and C atoms is expected to be through ionic bonds under these conditions. Charge transfer occurred during this process, while the graphene largely remained in its planar structure (Figure 5D). In order to validate this indication, we also calculated the peak area ratio of C−C sp^3 and sp^2

components by doing peak deconvolution. The sp^3/sp^2 ratio under this plasma condition (V_{dc} = 8 V) was determined to be only 0.06 (see Figure S1 in the Supporting Information). This is consistent with the above Raman results analysis. It is worth noting that this observation is similar to the predictions of some theoretical papers.[20,21] However, an important difference here is that the Cl coverage is high and therefore the distance between adjacent Cl atoms is small, while the "charge transfer complex" predicted in some theoretical papers[20,21] is for studying the case where a single Cl atom is absorbed on graphene, and thereby no Cl−Cl coupling needs to be considered.

At intermediate dc bias, for example at 16 V, the Raman D band was enhanced considerably. This indicates the introduction of broken symmetry in the graphene structure. There are two possible reasons for this symmetry-breaking: defect formation or an sp^2-to-sp^3 hybridization transition.[25,26] The difference is that the sp^2-to-sp^3 bonding type change is reversible under annealing, while the defect introductions are irreversible at an annealing temperature of 350 °C. Therefore, it indicates that the increased D peak mainly comes from the sp^2-to-sp^3 hybridization state transition (Figure 5E). By doing peak fitting, we also estimate that the XPS C 1s sp^3/sp^2 peak component ratio increased to 0.21:1 (see Figure S2 in the Supporting Information), which is much higher than the value of 0.06:1 when V_{dc} = 8 V. This is also consistent with the above analysis based on the Raman measurements. When the dc bias was further increased to 20 V, the D band increased significantly and became irreversible after annealing. In addition, a Raman D′ peak centered at 1620 cm^{-1} and a D+D′ peak at 2950 cm^{-1} began to develop after chlorination (Figure 5C). All of these symmetry-breaking Raman features indicate the onset of a defect creation process under this reaction condition[27] (Figure 5F). Future measurements using scanning tunneling microscopy and X-ray absorption and emission spectroscopy would help further investigate these indications of Cl−graphene interactions in the plasma environment.

Next, we investigated the uniformity of the chlorination process. A trapezoidally shaped exfoliated monolayer graphene flake (center of Figure 6A) was identified and confirmed by Raman characterization (Figure 6B). After chlorination, some Raman D band intensity developed (Figure 6C). Micro-Raman measurements revealed relatively uniform I_D/I_G and I_{2D}/I_G mapping results, as illustrated in Figure 6D and E. Since the spot size of the laser beam is about 1 μm, the plasma-based chlorination process is a uniform process on the scale of 1 μm.

DFT calculations predict that a band gap up to 1.21 eV can be opened when both sides of graphene are equally chlorinated and the C:Cl ratio reaches 1:1,[20] in which case the C:Cl on each single side would be 2:1. Our results on single-side chlorinated graphene will be useful for eventually achieving double-sided chlorinated graphene with C:Cl = 1:1. To explore this regime, we also fabricated suspended monolayer graphene devices and carried out temperature-dependent transport measurements to study the change in its band structure. So far, we have not observed clear evidence of a band gap.

CONCLUSIONS

In summary, we systematically investigated the plasma-based chlorination of graphene and characterized the resulting chlorinated graphene sample properties through Raman spectroscopy, XPS, and transport measurements. High surface coverage up to 45.3%, together with a high mobility of 1535 $cm^2/(V\ s)$, was achieved, and the chlorine coverage was finely tuned by controlling the plasma treatment time and dc bias.

Also, chlorinated graphene field-effect transistors were fabricated, and subsequent electronic characterization confirmed a hole doping effect and increased electrical conductivity. The interaction between C and Cl atoms can be quite distinctive under different dc bias conditions applied in the plasma chamber. Our results indicate that the conditions can be engineered to produce ionic bonding, covalent bonding (sp^2-to-sp^3 hybridization transition), and defect creation. Furthermore, the uniformity and reversibility of the chlorination process was also studied. It was demonstrated that chlorination in graphene *via* plasma reactions is a very effective and controllable way to engineer the structural and electronic properties of graphene. The high mobility of the resulting chlorinated graphene structures is a very important advantage of the Cl plasma approach relative to other functionalization approaches.

EXPERIMENTAL METHODS

Both exfoliated graphene flakes and large-area CVD-grown graphene were used as the host material. Graphene flakes exfoliated by micromechanical cleavage of highly ordered pyrolytic graphite (HOPG) were deposited on a silicon wafer containing a 300 nm SiO_2 layer on top.[1] Single-layer graphene areas were identified by optical microscopy and further confirmed by Raman spectroscopy.[28] The single-layer graphene was grown using a low-pressure (1.9 Torr) chemical vapor deposition method: copper foil was first annealed for 30 min at 1000 °C while flowing 10 sccm H_2, followed by 30 min growth in a mixed gas made of 4 sccm CH_4 and 70 sccm H_2.[29,30] The chlorine plasma treatments were performed in an electron cyclotron resonance reactive ion etcher (ECR/RIE, PlasmaQuest) running at a relatively low power. We carefully optimized both the ECR power and the dc bias to control the reaction conditions. Before each run, we used oxygen plasma to clean the chamber for 10 min. After that, the desired chlorine plasma recipe was run for another 10 min to properly condition the chamber, before treating the real graphene samples with the plasma.

The ECR power we used was 100 W. The flow rate of chlorine gas and pressure were maintained at constant values (flow rate: 80 sccm; pressure: 20 mTorr), and the Cl plasma temperature in our experiments was always kept at 25 °C.

Conflict of Interest: The authors declare no competing financial interest.

Supporting Information Available: Supplementary data of the deconvolution of the XPS C 1s spectra. This material is available free of charge *via* the Internet at http://pubs.acs.org.

Acknowledgment. We acknowledge partial support from the Army Research Laboratory grant W911NF-10-2-0049 and from the ONR GATE MURI program, monitored by Dr. Chagaan Bataar. We also appreciate the insightful discussions with Benjamin E. Feldman, Prof. Amir Yacoby, Paulo A. T. Araujo, and Joaquin R. Nieva.

REFERENCES AND NOTES

1. Novoselov, K. S.; Geim, A. K.; Morozov, S. V.; Jiang, D.; Zhang, Y.; Dubonos, S. V.; Grigorieva, I. V.; Firsov, A. A. Electric Field Effect in Atomically Thin Carbon Films. *Science* **2004**, *306*, 666–669.
2. Geim, A. K.; Novoselov, K. S. The Rise of Graphene. *Nat. Mater.* **2007**, *6*, 183–191.
3. Lee, C.; Wei, X.; Kysar, J. W.; Hone, J. Measurement of the Elastic Properties and Intrinsic Strength of Monolayer Graphene. *Science* **2008**, *321*, 385–388.
4. Elias, D. C.; Nair, R. R.; Mohiuddin, T. M. G.; Morozov, S. V.; Blake, P.; Halsall, M. P.; Ferrari, A. C.; Boukhvalov, D. W.; Katsnelson, M. I.; Geim, A. K.; *et al*. Control of Graphene's Properties by Reversible Hydrogenation: Evidence for Graphane. *Science* **2009**, *323*, 610–613.
5. Robinson, J. T.; Burgess, J. S.; Junkermeier, C. E.; Badescu, S. C.; Reinecke, T. L.; Perkins, F. K.; Zalalutdniov, M. K.; Baldwin, J. W.; Culbertson, J. C.; Sheehan, P. E.; *et al*. Properties of Fluorinated Graphene Films. *Nano Lett.* **2010**, *10*, 3001–3005.
6. Jeon, K.-J.; Lee, Z.; Pollak, E.; Moreschini, L.; Bostwick, A.; Park, C.-M.; Mendelsberg, R.; Radmilovic, V.; Kostecki, R.; Richardson, T. J.; *et al*. Fluorographene: A Wide Bandgap Semiconductor with Ultraviolet Luminescence. *ACS Nano* **2011**, *5*, 1042–1046.
7. Hong, X.; Cheng, S.-H.; Herding, C.; Zhu, J. Colossal Negative Magnetoresistance in Dilute Fluorinated Graphene. *Phys. Rev. B* **2011**, *83*, 085410.
8. Wang, B.; Sparks, J. R.; Gutierrez, H. R.; Okino, F.; Hao, Q.; Tang, Y.; Crespi, V. H.; Sofo, J. O.; Zhu, J. Photoluminescence from Nanocrystalline Graphite Monofluoride. *Appl. Phys. Lett.* **2010**, *97*, 141915–141915−3.
9. Balog, R.; Jørgensen, B.; Nilsson, L.; Andersen, M.; Rienks, E.; Bianchi, M.; Fanetti, M.; Lægsgaard, E.; Baraldi, A.; Lizzit, S.; *et al*. Bandgap Opening in Graphene Induced by Patterned Hydrogen Adsorption. *Nat. Mater.* **2010**, *9*, 315–319.
10. Cheng, S.-H.; Zou, K.; Okino, F.; Gutierrez, H. R.; Gupta, A.; Shen, N.; Eklund, P. C.; Sofo, J. O.; Zhu, J. Reversible Fluorination of Graphene: Evidence of a Two-Dimensional Wide Bandgap Semiconductor. *Phys. Rev. B* **2010**, *81*, 205435.
11. Shen, B.; Chen, J.; Yan, X.; Xue, Q. Synthesis of Fluorine-Doped Multi-layered Graphene Sheets by Arc-Discharge. *RSC Adv.* **2012**, *2*, 6761.
12. Chen, M.; Zhou, H.; Qiu, C.; Yang, H.; Yu, F.; Sun, L. Layer-Dependent Fluorination and Doping of Graphene *via* Plasma Treatment. *Nanotechnology* **2012**, *23*, 115706.
13. Lin, Y.-C.; Lin, C.-Y.; Chiu, P.-W. Controllable Graphene N-Doping with Ammonia Plasma. *Appl. Phys. Lett.* **2010**, *96*, 133110–133110−3.
14. Lu, Y. H.; Wu, R. Q.; Shen, L.; Yang, M.; Sha, Z. D.; Cai, Y. Q.; He, P. M.; Feng, Y. P. Effects of Edge Passivation by Hydrogen on Electronic Structure of Armchair Graphene Nanoribbon and Band Gap Engineering. *Appl. Phys. Lett.* **2009**, *94*, 122111–122111−3.
15. Sofo, J. O.; Chaudhari, A. S.; Barber, G. D. Graphane: A Two-Dimensional Hydrocarbon. *Phys. Rev. B* **2007**, *75*, 153401.
16. Li, B.; Zhou, L.; Wu, D.; Peng, H.; Yan, K.; Zhou, Y.; Liu, Z. Photochemical Chlorination of Graphene. *ACS Nano* **2011**, *5*, 5957–5961.
17. Wu, J.; Xie, L.; Li, Y.; Wang, H.; Ouyang, Y.; Guo, J.; Dai, H. Controlled Chlorine Plasma Reaction for Noninvasive Graphene Doping. *J. Am. Chem. Soc.* **2011**, *133*, 19668–19671.
18. Vinogradov, N. A.; Simonov, K. A.; Generalov, A. V.; Vinogradov, A. S.; Vyalikh, D. V.; Laubschat, C.; Mårtensson, N.; Preobrajenski, A. B. Controllable P-Doping of Graphene on Ir(111) by Chlorination with $FeCl_3$. *J. Phys.: Condens. Matter* **2012**, *24*, 314202.
19. Gopalakrishnan, K.; Subrahmanyam, K. S.; Kumar, P.; Govindaraj, A.; Rao, C. N. R. Reversible Chemical Storage of Halogens in Few-Layer Graphene. *RSC Adv.* **2012**, *2*, 1605–1608.
20. Şahin, H.; Ciraci, S. Chlorine Adsorption on Graphene: Chlorographene. *J. Phys. Chem. C* **2012**, *116*, 24075–24083.
21. Yang, M.; Zhou, L.; Wang, J.; Liu, Z.; Liu, Z. Evolutionary Chlorination of Graphene: From Charge-Transfer Complex to Covalent Bonding and Nonbonding. *J. Phys. Chem. C* **2012**, *116*, 844–850.
22. Subrahmanyam, K. S.; Voggu, R.; Govindaraj, A.; Rao, C. N. R. A Comparative Raman Study of the Interaction of Electron Donor and Acceptor Molecules with Graphene Prepared by Different Methods. *Chem. Phys. Lett.* **2009**, *472*, 96–98.
23. Lide, D. R. *CRC Handbook of Chemistry and Physics.: A Ready-Reference Book of Chemical and Physical Data*; CRC Press, 2004.
24. Ashcroft, N. W.; Mermin, N. D. *Solid State Physics*; Saunders College , 1976.
25. Ferrari, A. C. Raman Spectroscopy of Graphene and Graphite: Disorder, Electron−Phonon Coupling, Doping and Nonadiabatic Effects. *Solid State Commun.* **2007**, *143*, 47–57.
26. Malard, L. M.; Pimenta, M. A.; Dresselhaus, G.; Dresselhaus, M. S. Raman Spectroscopy in Graphene. *Phys. Rep.* **2009**, *473*, 51–87.
27. Dresselhaus, M. S.; Jorio, A.; Hofmann, M.; Dresselhaus, G.; Saito, R. Perspectives on Carbon Nanotubes and Graphene Raman Spectroscopy. *Nano Lett.* **2010**, *10*, 751–758.
28. Ferrari, A. C.; Meyer, J. C.; Scardaci, V.; Casiraghi, C.; Lazzeri, M.; Mauri, F.; Piscanec, S.; Jiang, D.; Novoselov, K. S.; Roth, S.; *et al*. Raman Spectrum of Graphene and Graphene Layers. *Phys. Rev. Lett.* **2006**, *97*, 187401.
29. Reina, A.; Jia, X.; Ho, J.; Nezich, D.; Son, H.; Bulovic, V.; Dresselhaus, M. S.; Kong, J. Large Area, Few-Layer Graphene Films on Arbitrary Substrates by Chemical Vapor Deposition. *Nano Lett.* **2009**, *9*, 30–35.
30. Li, X.; Cai, W.; An, J.; Kim, S.; Nah, J.; Yang, D.; Piner, R.; Velamakanni, A.; Jung, I.; Tutuc, E.; *et al*. Large-Area Synthesis of High-Quality and Uniform Graphene Films on Copper Foils. *Science* **2009**, *324*, 1312–1314.